Development of probability density functions for future South American rainfall

Tim E. Jupp[1], Peter M. Cox[1], Anja Rammig[2], Kirsten Thonicke[2], Wolfgang Lucht[2], Wolfgang Cramer[2]

[1] Mathematics Research Institute, University of Exeter, Exeter, Devon EX4 4QF, UK

[2] Potsdam Institute for Climate Impacts Research, D-14412 Potsdam, Germany

June 3, 2010

Word count (total): 4135
Word count (Introduction): 832
Word count (Description): 1699
Word count (Results): 1121
Word count (Discussion): 432
Word count (Acknowledgements): 51
Number of figures: 8
Number of tables: 4

Summary

- We estimate Probability Density Functions (PDFs) for future rainfall in five regions of South America, by weighting the predictions of the 24 CMIP3 General Circulation Models (GCMs). The models are rated according to their relative abilities to reproduce the inter–annual variability in seasonal rainfall.
- The relative weighting of the climate models is updated sequentially according to Bayes' theorem, based on the biases in the mean of the predicted time–series and the distributional fit of the bias–corrected timeseries.
- Depending on the season and the region, we find very different rankings of the GCMs, with no one model doing well in all cases. However in some regions and seasons, differential weighting of the models leads to significant shifts in the derived rainfall PDFs.
- Using a combination of the relative model weightings for each season we have also derived a set of overall model weightings for each region, which can be used to produce PDFs of forest biomass from the simulations of the Lund–Potsdam–Jena Dynamic Global Vegetation Model for managed land (LPJmL).

Key words: Amazonia, forest dieback, Climate change, Vegetation modelling, Probability, Bayesian statistics

1 Introduction

The Amazonian rainforest plays a crucial role in the climate system. It helps to drive atmospheric circulations in the tropics by absorbing energy and by recycling about half of the

rainfall that falls upon it. Furthermore, the region is estimated to contain about 10% of the carbon stored in land ecosystems, and to account for 10% of global net primary productivity (Melillo *et al.*, 1993). Despite large-scale human-deforestation, it seems likely that the region is currently acting as a net sink for anthropogenic CO_2 emissions (Tian *et al.*, 2000; Phillips *et al.*, 2009). The resilience of the forest to the combined pressures of deforestation and climate change is therefore of great concern, especially since at least one major climate model predicts a severe drying of Amazonia in the 21st century (Cox *et al.*, 2000, 2004).

Rainfall in Amazonia is sensitive to seasonal, interannual and decadal variations in sea-surface temperatures (Marengo, 2004; Fu *et al.*, 2001; Liebmann & Marengo, 2001). The warming of the tropical East Pacific during El Niño events suppresses wet-season rainfall through modification of the (East–West) Walker Circulation and via the Northern hemisphere extra-tropics (Nobre & Shukla, 1996). El Niño-like climate change (Meehl & Washington, 1996) has similarly been shown to influence annual mean rainfall over South America in General Circulation Model (GCM) climate change projections (Cox *et al.*, 2004; Li *et al.*, 2006). Variations in Amazonian precipitation are also known to be linked to sea–surface temperatures (SSTs) in the tropical Atlantic (Liebmann & Marengo, 2001). A warming of the tropical north Atlantic relative to the south leads to a north–westward shift in the Intertropical Convergence Zone (ITCZ) and compensating atmospheric descent over Amazonia (Fu *et al.*, 2001). For north–east Brazil the relationship between the north–south Atlantic SST gradient and rainfall is sufficiently strong to form the basis for a seasonal forecasting system (Folland *et al.*, 2001). The variations in SSTs in the tropical Atlantic and Pacific contribute in different ways to rainfall variability in the regions of Amazonia.

Despite this developing understanding of the dynamics of tropical climate variability and change, the current generation of GCMs give very different projections of future Amazon rainfall (Li *et al.*, 2006), varying from significant increases in rainfall to potentially damaging drying (Cox *et al.*, 2004). Figure 1 compares the simulated 20th century rainfall to the trend predicted for the 21st century for each of the 24 climate models available in the archive of the *Coupled Model Intercomparison Archive Project (CMIP3)*, and for the five regions of South America defined in Table 1. There is no clear consensus on rainfall change in any of the regions, with predicted trends in 21st century rainfall ranging from an increase of about +1 mm day^{-1} century^{-1} (e.g., model *o* in the EA and NEB regions) to a drying of -2 mm day^{-1} century^{-1} (e.g., model *w* in the EA region). More importantly, there is no obvious relationship between the ability of a given model to simulate the annual mean 20th century rainfall and the sign of its predicted trend in the future. For example, models with relatively realistic simulation of annual mean rainfall in Southern Amazonia (Figure 1(d)) include the models with the largest increases and decreases in the 21st century (models *r* and *w* respectively).

How can we help to inform decision-making given this uncertainty? One way is to weight the various model projections based on the ability of each model to produce key aspects of the observed climate. In this way we might hope to find more robust predictions by emphasizing the results from more realistic models and de-emphasizing the results produced by less realistic models. The method that we describe here is to construct a probabilistic prediction based on a *weighted* sum of the predictions of individual GCMs, using a Bayesian approach (Min *et al.*, 2007; Tebaldi & Knutti, 2007; Tebaldi & Sansó, 2009). The weight assigned to each GCM will be referred to as *the probability of the model* and will generate a probability density function (PDF) over the set of models. Bayes' theorem allows the model probabilities to be modified each time we consider the ability of the models to simulate some relevant aspect of current climate (such as seasonal rainfall) by comparing time–series of past observations with time-series of model simulations. In this study we weight models based on their ability to simulate both the mean state and the inter–annual variability (i.e. the statistical distribution) of current climate. In other words, the aim is to downweight those models whose mean value is far from the observed mean, or whose inter–annual variability is a poor fit to the observed distribution,

even when any bias in the mean value has been corrected.

The procedure can be summarised as follows:

(i) assign equal probability to all models - a *uniform prior* PDF.

(ii) choose a climatic variable of interest (in this case precipitation).

(iii) update the model PDF based on the fit between model simulations and observations for this variable.

(iv) use this posterior PDF to weight the predictions from individual models.

We make use of this procedure to estimate PDFs for future rainfall in each of the five regions of South America (Table 1; Figure 2), using rainfall simulations produced by the 24 CMIP3 GCMs (Table 2). In Section 2 we outline the theory and data on which our approach is based, and in Section 3 we discuss the PDFs for future rainfall that this procedure yields.

2 Description

2.1 Assigning Bayesian probabilities to climate model projections

In this section, we describe formally the procedure that we have adopted. We consider the case in which there are $N = 24$ climate models (Table 2), denoted alphabetically by the labels $m_1 = a$ to $m_N = x$. For each of the five regions listed in Table 1, the aim is to assign a probability to the i'th model based on its ability to simulate the seasonal precipitation observed in the twentieth century. In the absence of any other information about the performance of the models it is natural to assign equal weight to each of them. In the language of Bayesian statistics, we therefore assign a *uniform prior distribution* to the models

$$\pi(m_i) = \frac{1}{N}, \quad \forall i \in \{1, 2, \ldots, N\} \tag{1}$$

In other words, the *prior probability* of the i'th model is set to be $1/N$. A naïve multi–model prediction would simply combine the predictions from individual models according to this uniform prior. The salient feature of our method is that predictions for the twenty–first century will be created by assigning different weights to different model predictions according to the models' performance in the twentieth century.

Having assigned a prior PDF, the next step is to assess the performance of each model over the historical period. This is accomplished by comparing time–series from observations with model simulations over the historical period. For example, Figure 3a compares observations of twentieth century annual–mean rainfall in Eastern Amazonia (solid line) with annual–mean rainfall simulated by the 24 climate models (grey) listed in Table 2. Data are presented in the form of time–averages taken over the calendar year January–December ('ann'). It follows that our measure of statistical variability is the inter–annual variability in annual–mean rainfall.

Several important points are illustrated by Figure 3a. Firstly, no climate model is able to simulate exactly the observed year–to–year variability in rainfall. In other words, the peaks and troughs of the solid line (observations) do not coincide with the peaks and troughs of any of the grey lines (the raw simulations from the 24 models). This is a function of the chaotic nature of the climate system and is both unavoidable and entirely expected. The best we can demand from a climate model is that it should simulate well the observed *statistical distribution* of any climate variable over a period of a few decades (or, in this example, the twentieth century).

It is clear from Figure 3a that none of the models captures the observed distribution well. Consider first of all the century–mean of all of the time-series. It is clear that most of the

century–means of the simulations $\langle r_{i,t} \rangle$ are lower than the century–mean of the observations $\langle o_t \rangle = 6.05$ mm day^{-1}. (We use angle brackets to denote a temporal average over the twentieth century.) This is an illustration of *bias* in the models. To remove this bias, it is standard practice to perform some sort of bias correction to the model simulations so that the long–term mean value of the simulated climate variable agrees with observations. The precise way in which model simulations are corrected for bias will be discussed further in Section 3.1. In Section 2.2, we will discuss the way in which models with greater bias will be assigned a lower weighting in the model PDF.

Figure 3a illustrates that the century–means of the bias–corrected simulations $\{\langle b_{i,t} \rangle\}$ are all – as expected – closer than the raw simulations to the century–mean of the observations $\langle o_t \rangle = 6.05$ mm day^{-1}. It is still possible, however, to discriminate amongst the (bias–corrected) models by assessing how well the distributions of the bias–corrected simulations fit the distribution of the observations. This point is illustrated in Figure 3b. Here, the empirical cumulative distribution functions (CDFs) of the raw simulations $\{r_{i,t}\}$ (grey), bias–corrected simulations $\{b_{i,t}\}$ (dashed) and observations $\{o_t\}$ (solid) are compared. It is clear that the bias–corrected simulations (dashed) have CDFs that are 'closer' to the observations (black) than the raw simulations (grey). We will show below, in Section 2.3, how models whose CDFs are 'closest' to the observations will receive highest weighting in our model PDF.

In particular we wish to assign greater weight to those models that simulate well the observed inter–annual variability in seasonal rainfall. For each spatial region and for each season, the model PDF is updated in a two–stage process. Firstly, the climate prediction index C described in Section 2.2 is used to assess the degree to which the mean of the raw simulations of the i'th model, $\langle \{r_{i,t}\} \rangle$ fits the mean of the observations $\langle o_t \rangle$. Secondly, the Kolmogorov–Smirnov statistic D described in Section 2.3 is used to assess the similarity of the distribution of bias–corrected simulations of the i'th model, $\{b_{i,t}\}$ to the distribution of the observations $\{o_t\}$.

In general terms, the sequential modification of the model PDF proceeds by considering the likelihood $f(d|m_i)$ of observed data d under the assumption that model m_i is correct. The posterior PDF is calculated from the prior PDF by Bayes' formula

$$p(m_i) \propto f(d|m_i)\pi(m_i) \tag{2}$$

with an appropriate normalisation being applied so that $\sum_{i=1}^{N} p(m_i) = 1$.

In the next two sections we outline plausible forms for the likelihood function $f(d|m_i)$ to assess the bias of the raw simulations $\{r_{i,t}\}$ and the distributional fit to the data of the bias–corrected simulations $\{b_{i,t}\}$.

Since rainfall must be non–negative we apply a logarithmic transformation to obtain the bias–corrected rainfall simulations. Specifically, the bias–corrected rainfall simulations are constructed according to the following formula:

$$\log b_{i,t} = \log r_{i,t} - \langle \log r_{i,t} \rangle + \langle \log o_t \rangle \tag{3}$$

where the angle brackets denotes a temporal mean over the twentieth century.

2.2 A measure for bias: the climate prediction index C

Here we consider how to weight the climate models according to the mean bias in the raw simulations $\{r_{i,t}\}$. For this we compare the century–mean of the observations $\langle o_t \rangle$ with the century–mean of the i'th (raw) model simulation $\langle r_{i,t} \rangle$. We construct the sample variance σ^2 of the century–mean amongst the different models

$$\sigma^2 = \frac{1}{N-1} \sum_{n=1}^{N} \left(\langle r_{i,t} \rangle - \frac{1}{N} \sum_{n=1}^{N} \langle r_{i,t} \rangle \right)^2 \tag{4}$$

Following (Murphy *et al.*, 2004) we then construct a climate–prediction index

$$C_i = \left(\langle r_{i,t} \rangle - \langle o_t \rangle\right)^2 \tag{5}$$

as a measure of the bias of the i'th model. The corresponding likelihood of the data d (which in this case is the climate prediction index C_i) is then assumed (Murphy *et al.*, 2004) to take the functional form

$$f(d|m_i) = \exp\left(-\frac{C_i}{2\sigma^2}\right) \tag{6}$$

2.3 A measure for distributional fit: The Kolmogorov–Smirnov statistic D

Here we consider how to rate the climate models according to the shape of the distribution of the bias–corrected simulations $\{b_{i,t}\}$. In order to compare the distributions of the bias–corrected simulations $\{b_{i,t}\}$ and the observations $\{o_t\}$ we consider empirical cumulative distribution functions (CDFs) as shown in Figure 4a. The CDF $F(x)$ of a variable x is simply the proportion of the data whose value is less than or equal to x. Suppose that the observations consist of a time–series of length n_0, while the bias–corrected simulation from the i'th model consists of a time–series of length n_i. (In the example that we present in Section 3.1, the data cover the years 1901 – 1999 and so $n_0 = n_i = 99$.) We construct empirical CDFs $F_0(x)$ and $F_i(x)$ for the two time–series and compare them. Clearly, a good model is one whose CDF $F_i(x)$ is reasonably 'close' to the CDF of the observations $F_0(x)$. A standard measure of the closeness of two distributions, whose distribution is easily calculated, is the Kolmogorov–Smirnov statistic D defined by

$$D_i = \max |F_0(x) - F_i(x)| \tag{7}$$

Thus, for each model m_i we can regard D_i as a measure of the difference between the CDF of the (bias–corrected) simulations of the i'th model and the CDF of the observations. The distribution $f_{KS}\left(D_i; n_0, n_i\right)$ of the Kolmogorov–Smirnov statistic D can be calculated under the null hypothesis that the observations and the simulation are drawn from the same distribution. This distribution is known as the Kolmogorov distribution and it is easily calculated by standard statistical software packages (given knowledge of the two sample sizes n_0 and n_i) as a function of D_i. The PDF of the Kolmogorov distribution with $n_0 = n_i = 99$ is shown in Figure 4b.

It follows that the likelihood of the data d (which in this case is the Kolmogorov–Smirnov statistic D_i) under model m_i is

$$f(d|m_i) = f_{KS}\left(D_i; n_0, n_i\right) \tag{8}$$

2.4 Data

Two types of data are used in this study – observational data for the twentieth century alone and model–based data for the twentieth and twenty–first centuries. The data taken to represent the 'true' state of the climate are taken from the CRU TS 3.0 archive. These data are available at `http://www.cru.uea.ac.uk/cru/data/hrg-interim/`. GCM data are taken from the CMIP3 multi–model archive, in the Climate of the 20th Century experiment. There are 24 models, listed in Table 2. These data are available at `https://esg.llnl.gov:8443/`.

For assessment of 20th century climate, raw data consist of monthly averages for the period January 1901 – December 1999 (this is the longest period for which data are available from all sources.) Similarly, model predictions for the twenty–first century are considered at a monthly resolution for the period January 2001 – December 2098. For the analysis, five types of seasonal average were created by averaging over the periods January–December (denoted by 'ann'), December–February ('DJF'), March–May ('MAM'), June–August ('JJA') and September–November ('SON'). The final time–series used in the analysis were then obtained by taking spatial averages of these seasonal data in a total of five spatial windows (Table 1).

2.5 Validation

It is important to assess whether or not the posterior weighting of the GCMs can be said to produce 'better' predictions of a climate variable x than simple uniform prior weighting via equation 1. To test this, we split the data from the twentieth century into a training period covering the years 1901–1959 and a validation period covering the years 1960–1999. For a climate variable x, model weights (both the uniform prior weights and the posterior weights obtained by considering the observations in the training period) can be used to produce a predicted CDF $F(x)$ for the validation period. The difference between the predicted CDF $F(x)$ and the observed CDF $F_0(x)$ in the validation period is then quantified by the root–mean–square-error E:

$$E = \sqrt{\frac{1}{x_2 - x_1} \int_{x_1}^{x_2} \left(F(x) - F_0(x)\right)^2 \, \mathrm{d}x} \tag{9}$$

Clearly, it is desirable that the values of E for posterior–weighted predictions be less than those for prior–weighted predictions.

3 Results

In this section we present detailed results for one illustrative region and season (Section 3.1) before summarising our results for the remaining cases (Section 3.2). All calculations reported here were performed using the statistical package `R`. We have chosen this software because it is both powerful and freely available for download[1]. The results reported here were produced by an `R`–code that we have written specifically for the purpose of Bayesian reweighting of climate model predictions.

3.1 Example: annual–mean rainfall in Eastern Amazonia

We report the steps below sequentially but stress that the same final result would be obtained if the data constraints were considered in a different order.[2]

By definition, our initial model PDF for the $N = 24$ models is the uniform prior (equation 1). We will now modify this PDF according to the models' ability to simulate annual–mean rainfall in Eastern Amazonia over the twentieth century.

3.1.1 Bias in the raw simulations

Raw simulations of annual–mean rainfall $\{r_{i,t}\}$ in Eastern Amazonia are shown in grey in Figure 3a. The century mean rainfall simulated by the i'th model $\langle r_{i,t} \rangle$ is compared with the century–mean of the observations $\langle o_t \rangle = 6.05$ mm day^{-1} via equations 4 and 5. Equation 6 then yields the likelihood of the data under each of the models. This likelihood is shown for each model in Figure 5a. The likelihood is then combined with the (uniform) prior via equation 2 to yield the model PDF shown in Figure 5b. The dashed horizontal line in this and subsequent figures for model PDFs denotes the uniform PDF for reference.

3.1.2 Distributional shape of the bias–corrected simulations

The next stage of the process is to modify the current model PDF (in Figure 5b) according to the (bias–corrected) models' ability to simulate the distribution of annual–mean rainfall when bias–corrected by equation 3. The distribution of the bias–corrected simulations (Figure 3b,

[1] available at http://cran.r-project.org/

[2] The insensitivity to ordering comes from the fact that at each stage the PDF is modified by a multiplication, and of course a multi–stage multiplication can be performed in any order.

dashed lines) is then compared with the distribution of the observations (Figure 3b, black lines) using the Kolmogorov–Smirnov statistic (equation 7). Finally, equation 8 yields the likelihood of the data under each of the models as shown in Figure 5d. This likelihood is combined with a prior taken from the previous calculation (i.e. the model PDF in Figure 5b) via Bayes' theorem (equation 2) to yield the updated model PDF shown in Figure 5e,f. It is clear that the simulated interannual variability discriminates much more clearly between different models than the simulated mean rainfall, such that the final model PDF is dominated by this stage of the procedure.

3.1.3 PDF for future rainfall

We are now in a position to calculate a probability distribution for future rainfall by weighting the predictions of individual models. It is important that some models predict a downward trend in rainfall while others predict little trend or indeed an upward trend (Li *et al.*, 2006). Our final estimate of the trend in twenty–first century rainfall will of course depend on how the model PDF (Figure 5e,f) distributes probability weight between models with upward and downward trend.

Figure 6a shows model predictions of annual–mean rainfall in the early part of the twenty–first century (2001-2031). The predictions from individual climate models are shown as grey lines. These curves are cumulative distribution functions (CDFs) of the (bias–corrected) rainfall predicted by each of the $N = 24$ CMIP3 climate models. These individual predictions have then been combined using the model PDF of Figure 5e,f to give an overall distribution for rainfall that is a weighted average across models. This distribution is shown in black, and represents our final probabilistic prediction based on the criteria that we have outlined above.

We now consider how the predicted rainfall changes from the beginning to the end of the twenty–first century. Figure 6b shows model predictions of climate in the last thirty years of the twenty–first century. Again, the predictions of the individual climate models are shown as grey lines and a weighted average using the model PDF of Figure 5d,e is shown in black.

Figure 6c illustrates the change in model–weighted rainfall predictions between the period 2001–2031 and the period 2068–2098. It is clear that the spread of the probabilistic prediction increases over the twenty–first century. This is a consequence of the prediction being an average across all models. Over the 21st century, some of the models predict increased rainfall while others predict decreased rainfall (Li *et al.*, 2006). Thus, unless all models of one 'sign' are very significantly downweighted in the model PDF, the weighted–average rainfall prediction must assign some probability to increased rainfall and some probability to decreased rainfall. We can essentially discount the possibility of 'very high' or 'very low' rainfall in the early 21st century (Figure 6a) because there are no models that predict these extreme values. For the late 21st century, however, we cannot rule out 'very high' or 'very low' rainfall (Figure 6b) because (a) some models predict high rainfall and some models predict low rainfall and (b) the evidence does not lead to significant downweighting of all 'low' models or all 'high' models.

Figure 6c contains cumulative distribution functions (CDFs). For ease of interpretation these functions may be differentiated to obtain probability density functions (PDFs) for future rainfall. The PDFs for all regions are shown in Figure 7 and show the change in predicted rainfall PDF between the period 2001–2031 and the period 2068–2098. In the case of Eastern Amazonia (Figure 7a) our results suggest that a 'low' annual–mean rainfall of about 3 mm day^{-1} is much more likely to occur at the end of the twenty–first century than at the beginning of the twenty–first century.

3.2 Results for other regions and seasons

We compared observed and simulated annual mean rainfall in the 20th century for the five study regions. In general, there are systematic errors in rainfall, with climate models tending to overestimate rainfall in Northeastern Brazil but underestimate rainfall in the other four regions.

Figure 8 contains the results of the validation procedure described in Section 2.5. The posterior–weighted predictions perform better than the prior–weighted predictions in most cases and perform only slightly worse in the remainder.

We repeat the Bayesian weighting procedure for each of the five regions in Table 1. In each case we make use of both the bias in the mean rainfall (via the index C), and the Kolmogorov–Smirnov statistic of the bias–corrected rainfall (via the index D), to downweight the models. Table 3 shows the relative model weightings derived for each region which result from considering annual mean rainfall. These overall weightings were subsequently used to produce PDFs of biomass change from the forest projections produced by the LPJ model (Rammig *et al.*, 2010).

4 Discussion

It is clear that the relative ranking of GCMs varies significantly with region and season. In any one region it is also unusual for a given model to simulate rainfall accurately in all four seasons. As a result models that do simulate each season well tend to dominate the overall weighting (e.g. models p and q in Eastern Amazonia, model h in North–East Brazil, models p and s North–West Amazonia, models h and s in Southern Brazil).

As an indication of the risk of drought, the probability of annual rainfall being less than 3 mm day^{-1} was also calculated for each of the five regions. The results are summarized in Table 4 and indicate an estimated six-fold increase by the end of the twenty–first century in the likelihood of drought-like conditions for Southern Brazil, and smaller increases for Eastern and Southern Amazonia.

To summarise, we have estimated Probability Density Functions (PDFs) for future rainfall in five regions of South America, by weighting the predictions of the 24 CMIP3 General Circulation Models (GCMs) according to their relative abilities to reproduce the mean and variability of the observed rainfall in each season. The relative weighting of the climate models was updated sequentially according to Bayes' theorem, based on the biases in the mean rainfall and the distributional fit of the bias-corrected timeseries as measured by the Kolmogorov–Smirnov statistic, D. Using a combination of the relative model weightings for each season, we have also derived a set of overall model weightings for use by the PIK–LPJ group (Rammig *et al.*, 2010).

Depending on the season and region, we find very different rankings of the GCMs, with no one model doing well in all cases. However in some regions posterior weighting of the models leads to significant shifts in the derived rainfall PDFs between the beginning and end of the 21st century, including a significant increase in the risk of annual mean rainfall below 3 mm day^{-1} in Southern Brazil. Compared to a method in which models are simply weighted equally, the Bayesian approach adopted here provides an estimate of future rainfall in Amazonia that makes greater use of the information available in the historical record. There are still, however, very significant uncertainties associated with deficiencies in GCM rainfall simulation in this region. In the future, the Bayesian methodology described here could be adapted to incorporate statistical descriptions of the uncertainty present in the historical record and a multivariate assessment of model performance. It could also be used to assess GCMs based on their ability to reproduce other variables known to be climatically significant such as regional sea–surface temperatures.

Acknowledgements

This work was funded by World Bank Grant "Assessment of the prospects and identification of the implications of Amazon dieback induced by climate change" (Contract no. 7146402). We thank Jose Marengo, Walter Vergara, Sebastian Scholz and Alejandro Deeb for fruitful discussions, and three anonymous referees for improving the quality of the manuscript.

References

Covey C, AchutaRao KM, Cubash C, Jones P, Lambert SJ, Mann ME, Phillips TJ, Taylor KE. 2003. An Overview of Results from the Coupled Model Intercomparison project (CMIP). *Global and Planetary Change* **37**: 103-133.

Cox PM, Betts RA, Jones CD, Spall SA, Totterdell IJ. 2000. Acceleration of global warming due to carbon cycle feedbacks in a coupled climate model. *Nature* **408**: 184–187.

Cox PM, Betts RA, Collins M, Harris PP, Huntingford C, Jones, CD. 2004. Amazonian forest dieback under climate–carbon cycle projections for the 21st century. *Theoretical and Applied Climatology*: doi:10.1007/s00704-004-0049-4.

Folland CK, Colman AW, Rowell DP, Davey MK. 2001. Predictability of Northeast Brazil rainfall and real–time forecast skill 1987-1998. *Journal of Climate* **14**: 1937-1958.

Fu R, Dickinson RE, Chen MX, Wang H. 2001. How do tropical sea surface temperatures influence the seasonal distribution of precipitation in the equatorial Amazon? *Journal of Climate* **14**: 4003-4026.

Li W, Fu R, Dickinson RE. 2006. Rainfall and its seasonality over the Amazon in the 21st century as assessed by the coupled models for the IPCC AR4. *Journal of Geophysical Research* **111**: doi:10.1029/2005JD006355.

Liebmann B, Marengo J. 2001. Interannual variability of the rainy season and rainfall in the Brazilian Amazon basin. *Journal of Climate* **14**: 4308-4318.

Marengo, JA. 2004. Interdecadal variability and trends of rainfall across the Amazon basin. *Theoretical and Applied Climatology* **78**: 79-96.

Meehl GA, Washington WM. 1996. El Niño-like climate change in a model with increased atmospheric CO2 concentrations. *Nature* **382**: 56-60.

Melillo JM, McGuire AD, Kicklighter DW, Moore III B, Vorosmarty CJ, Schloss AL. 1993. Global climate change and terrestrial net primary production. *Nature* **363**: 234-240.

Min S.-K., Simonis D, Hense A. 2007. Probabilistic climate change predictions applying Bayesian model averaging. *Philosophical Transactions of the Royal Society A* **365**: 2103-2116: 10.1098/rsta.2007.2070.

Murphy JM, Sexton DMH, Barnett DN, Jones GS, Webb MJ, Collins M, Stainforth DA. 2004. Quantification of modelling uncertainties in a large ensemble of climate change simulations. *Nature* **430**: 768 – 772.

New M, Hulme M, Jones P. 1999. Representing twentieth century space-time climate variability. 1: Development of a 1961-1990 mean monthly terrestrial climatology. *Journal of Climate* **12(3)**: 829–856.

New M, Hulme M, Jones, P. 2000. Representing twentieth–century space-time climate variability. Part II: Development of 190196 monthly grids of terrestrial surface climate. *Journal of Climate* **13**: 2217-2238.

Nobre P, Shukla J. 1996. Variations of sea surface temperature, wind stress and rainfall over the tropical Atlantic and South America. *Journal of Climate* **9**: 2464-2479.

Phillips, OL et al. 2009. Drought Sensitivity of the Amazon Rainforest. *Science* **323 (1344)**: 10.1126/science.1164033.

Rammig A, Thornicke K, Lucht W, Cramer W, Jupp TE, Cox PM. 2010. Estimating the risk of Amazonian Forest Dieback. *New Phytologist* **this issue**.

Rayner NA, Parker DE, Horton EB, Folland CK, Alexander LV, Rowell DP, Kent EC, Kaplan A. 2003. Global analyses of SST, sea ice and night marine air temperature since the late nineteenth century. *Journal of Geophysical Research* **108(D14)**: 10.1029/2002JD002670.

Tebaldi C, Knutti R. 2007. The use of the multi–model ensemble in probabilistic climate projections. *Philosophical Transactions of the Royal Society A* **365**: 2053-2075: 10.1098/rsta.2007.2076.

Tebaldi C, Sansó B. 2009. Joint projections of temperature and precipitation change from multiple climate models: a hierarchical Bayesian approach. *Journal of the Royal Statistical Society* **172**: 83-106.

Tian H, Melillo JM, Kicklighter DW, McGuire AD, Helfrich III J, Moore III B, Vorosmarty, CJ. 2000. Climatic and biotic controls on annual carbon storage in Amazonian ecosystems. *Global Ecology and Biogeography* **9**: 315-335.

Region	Identifier	longitude	latitude
Eastern Amazonia	EA	55^oW - 45^oW	5^oS - 2.5^oN
Northwest Amazonia	NWA	72.5^oW - 60^oW	5^oS - 5^oN
Northeast Brazil	NEB	45^oW - 35^oW	15^oS - 2.5^oS
Southern Amazonia	SAz	65^oW - 50^oW	17.5^oS - 10^oS
Southern Brazil	SB	60^oW - 45^oW	35^oS - 22.5^oS

Table 1: Definitions of the regions referred to in this study.

Model Identifier	Model Name	Model Identifier	Model Name
a	`bccr_bcm2_0`	m	`ingv_echam4`
b	`cccma_cgcm3_1`	n	`inmcm3_0`
c	`cccma_cgcm3_1_t63`	o	`ipsl_cm4`
d	`cnrm_cm3`	p	`miroc3_2_hires`
e	`csiro_mk3_0`	q	`miroc3_2_medres`
f	`csiro_mk3_5`	r	`miub_echo_g`
g	`gfdl_cm2_0`	s	`mpi_echam5`
h	`gfdl_cm2_1`	t	`mri_cgcm2_3_2a`
i	`giss_aom`	u	`ncar_ccsm3_0`
j	`giss_model_e_h`	v	`ncar_pcm1`
k	`giss_model_e_r`	w	`ukmo_hadcm3`
l	`iap_fgoals1_0_g`	x	`ukmo_hadgem1`

Table 2: Labelling of the climate models referred to in this study. The models are those in the World Climate Research Programme's (WCRP's) Coupled Model Intercomparison Project phase 3 (CMIP3) multi-model dataset in the "Climate of the 20th Century" experiment `https://esg.llnl.gov:8443/`.

	EA	NEB	NWA	SAz	SB
a	0.87	0.07	1.77	2.49	0.04
b	9.91	0.39	5.60	7.68	0.09
c	9.94	0.71	5.61	7.53	0.00
d	4.15	0.07	5.14	7.58	0.12
e	1.44	0.95	0.17	3.87	0.20
f	0.00	1.00	0.00	0.00	1.20
g	0.19	3.33	0.00	0.07	1.28
h	0.16	21.56	0.00	0.00	21.17
i	1.35	0.00	3.77	2.11	0.17
j	2.67	0.05	5.55	2.04	0.73
k	1.92	0.00	1.88	0.65	6.13
l	2.71	2.36	3.80	7.50	8.06
m	3.66	0.34	4.23	7.60	1.34
n	4.03	2.16	3.85	0.88	2.33
o	0.90	7.42	0.96	0.11	16.82
p	13.63	2.78	14.08	3.42	0.08
q	13.61	4.45	1.75	1.27	1.07
r	9.93	0.47	10.24	2.02	0.52
s	0.12	14.07	14.10	10.64	21.10
t	5.44	17.08	3.33	7.54	13.90
u	9.90	0.00	2.73	10.25	0.47
v	0.03	0.06	5.05	10.44	1.61
w	1.77	8.11	2.68	2.85	1.47
x	1.67	12.58	3.72	1.45	0.09

Table 3: Posterior probabilities (expressed as percentages) assigned to models of Table 2 in the regions of Table 1.

Region	Prior 2001-2031	Prior 2068-2098	**Posterior** 2001-2031	**Posterior** 2068-2098
Eastern Amazonia	0.6%	2.7 %	0 %	0.7 %
Northwest Amazonia	0 %	0 %	0 %	0 %
Northeast Brazil	86 %	80 %	80 %	76 %
Southern Amazonia	0.14 %	0.7 %	0 %	0.1 %
Southern Brazil	0.4 %	1.7 %	1.1 %	6.8 %

Table 4: Probability of annual rainfall being less than 3 mm day^{-1} for each of the five study regions of Amazonia. In each case probabilities are shown for the two periods, 2001-2031 and 2068-2098, and for the uniform prior distribution as well as the Bayesian posterior distribution. The posterior distributions represent 'best' estimates based on information currently available.

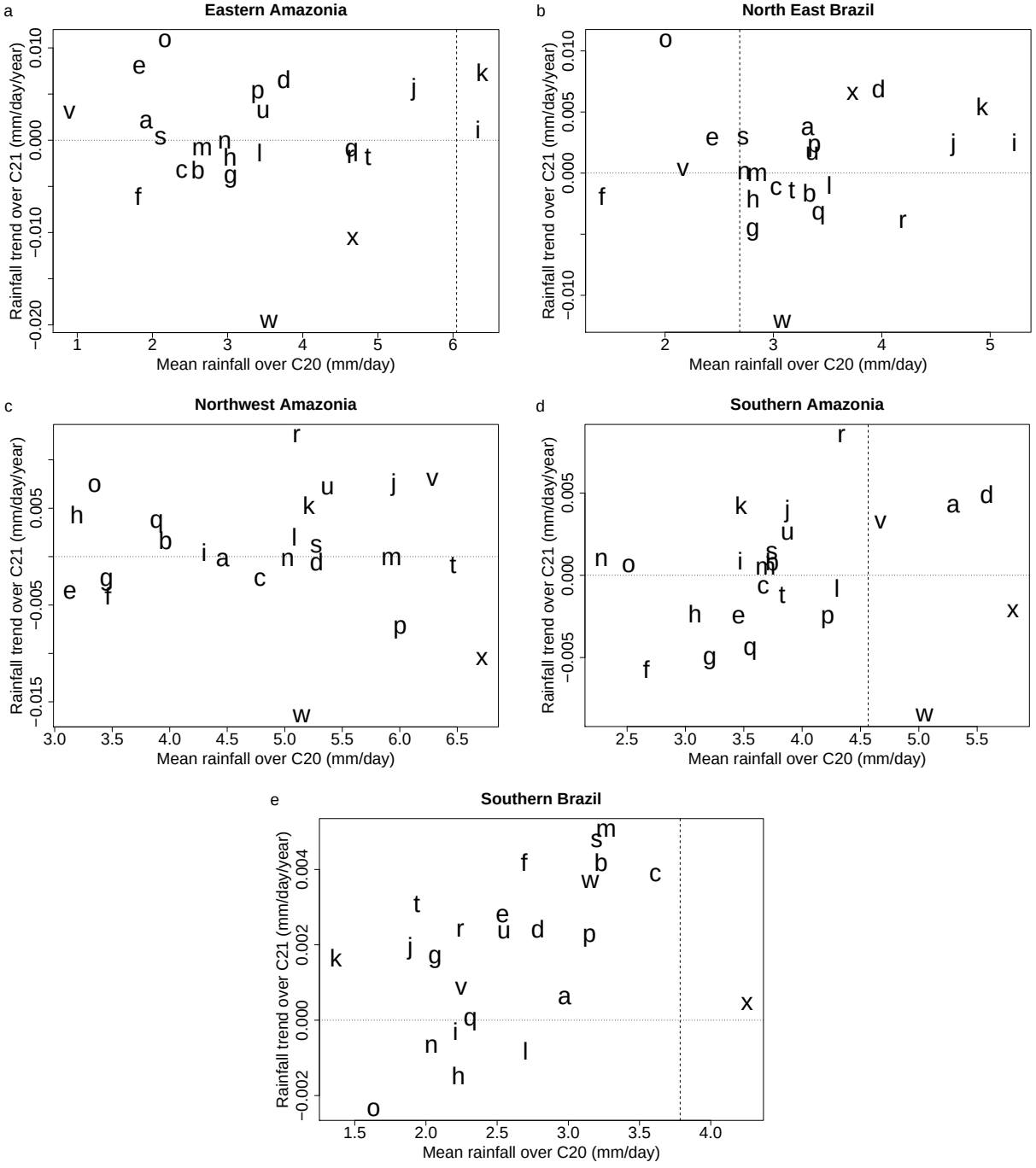

Figure 1: Annual means (twentieth century) and linear trends (twenty–first century) in each of the climate models listed in Table 2. Vertical line shows observed annual mean rainfall in twentieth century. Horizontal line separates models with positive trend from models with negative trend.

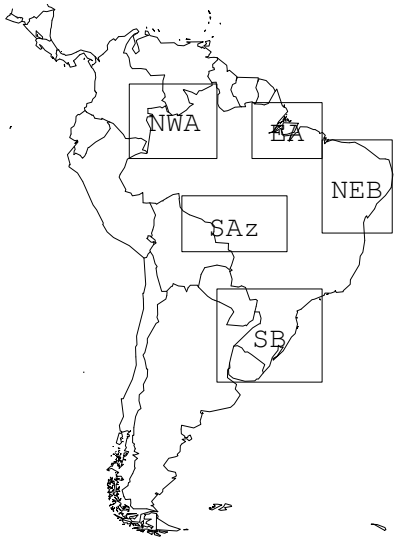

Figure 2: The regions defined in Table 1.

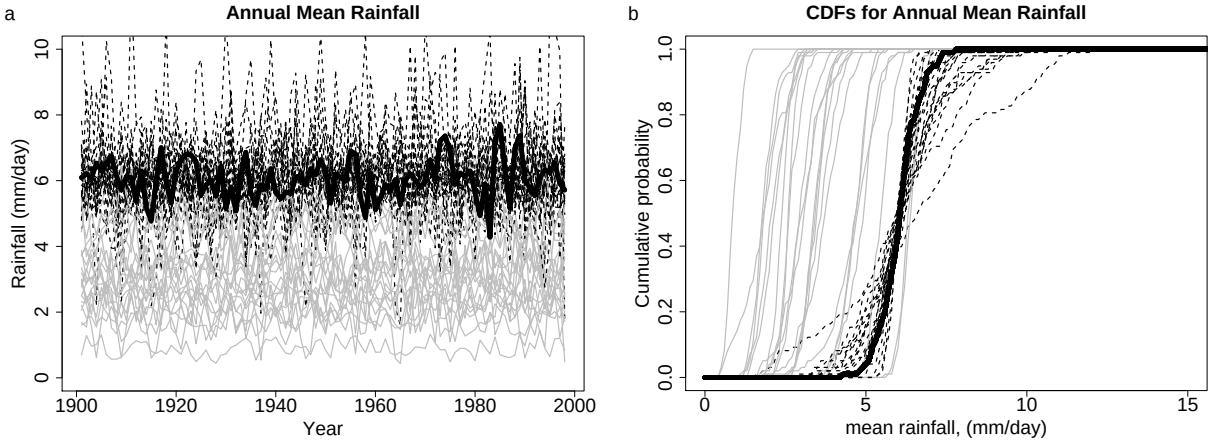

Figure 3: Time–series and associated cumulative distribution functions (CDFs) for the Eastern Amazonia region (Figure 2). Solid lines – observations $\{o_t\}$ from the CRU dataset, grey lines – (raw) climate model simulations $\{r_{i,t}\}$ from each of the climate models listed in Table 2, dashed lines – bias–corrected climate model simulations $\{b_{i,t}\}$ (equation 3) from each of the climate models. (a) Time–series data. (b) Empirical cumulative distribution functions (CDFs) corresponding to the time–series shown in (a).

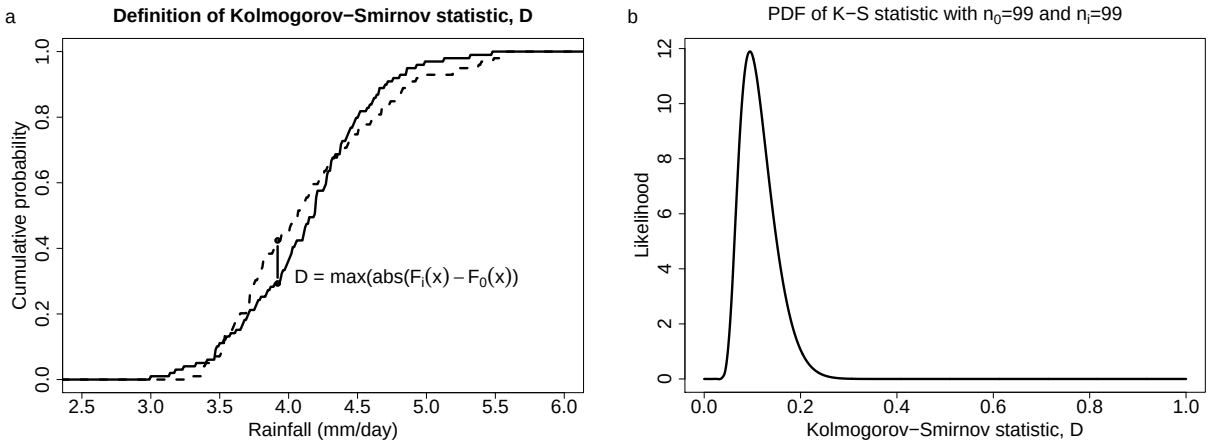

Figure 4: The Kolmogorov–Smirnov statistic as a measure of the difference between two cumulative distribution functions (CDFs). (a) The Kolmogorov–Smirnov statistic D_i is defined as the maximum difference between two CDFs, where the CDFs are derived from samples of size n_0 and n_i respectively. The two CDFs shown here are for illustrative purposes only and do not correspond to the data discussed in the text. (b) The probability density function (PDF) of D_i in the case when $n_0 = n_i = 99$ and the two samples are drawn from identical distributions.

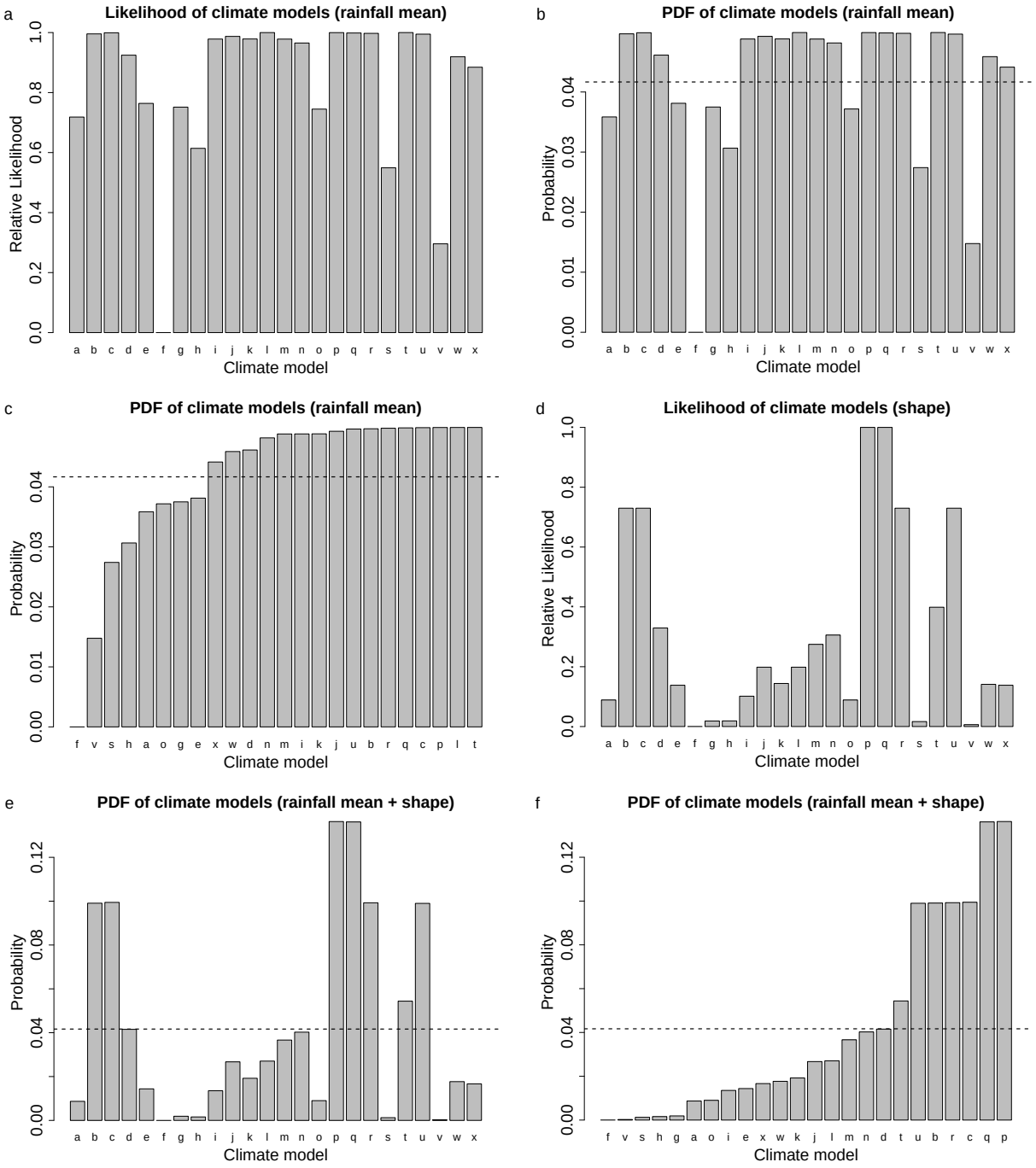

Figure 5: Steps in the calculation of a PDF across the $N = 24$ models, shown here for the illustrative case of annual–mean rainfall in Eastern Amazonia (Figure 3). Initially, a uniform prior (equation 1) is assigned across the models. (a) The likelihood of each model, calculated from equation 6, is a measure of each model's ability to reproduce the mean of the observed time–series. (b) Updated model PDF, incorporating the likelihood information in (b). Dashed horizontal line indicates prior probability $1/N$ initially assigned to each model. (c) The model PDF shown in (b), with models sorted into ascending order of probability. (d) The likelihood of each model, calculated from equation 8, is a measure of each model's ability (after bias–correction) to reproduce the distributional shape of the observed time–series. (e) Updated model PDF, incorporating the likelihood information in (d). (f) The model PDF shown in (e), with models sorted into ascending order of probability.

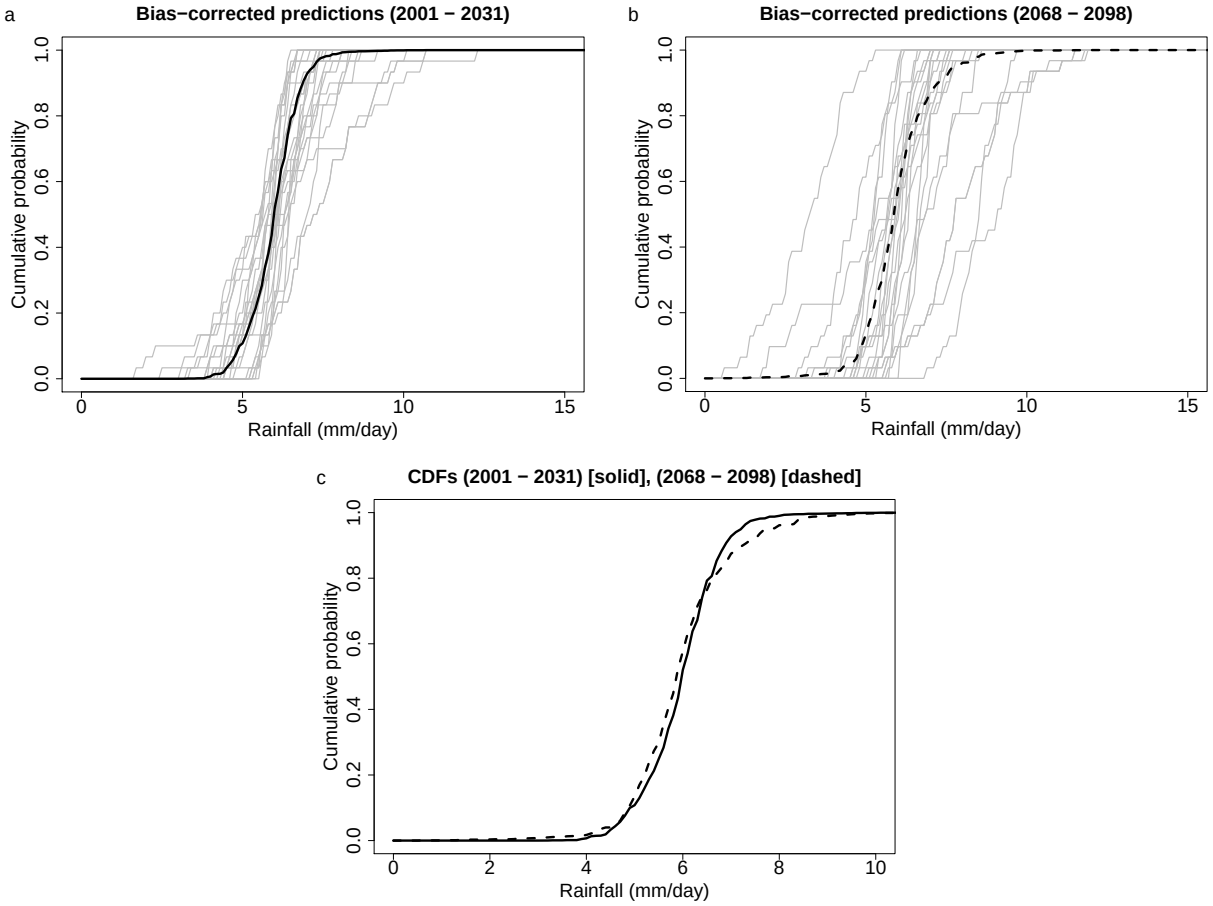

Figure 6: Predictions of twenty–first century annual–mean rainfall in Eastern Amazonia (Li *et al.*, 2006). (a) CDFs of predicted rainfall in the period 2001–2031. Grey – the predictions of each of the $N = 24$ models. Solid black – combined prediction, obtained by weighting each model with the model probabilities in Figure 5e. (b) CDFs of predicted rainfall in the period 2068–2098. Grey – the predictions of each of the $N = 24$ models. Dashed black – combined prediction, obtained by weighting each model with the model probabilities in Figure 5e. (c) Comparison of the weighted predictions for early and late twenty–first century (PDFs corresponding to these CDFs are shown in Figure 7a). Grey – observed distribution in twentieth century. Solid – predicted distribution in early twenty–first century. Dashed – predicted distribution in late twenty–first century.

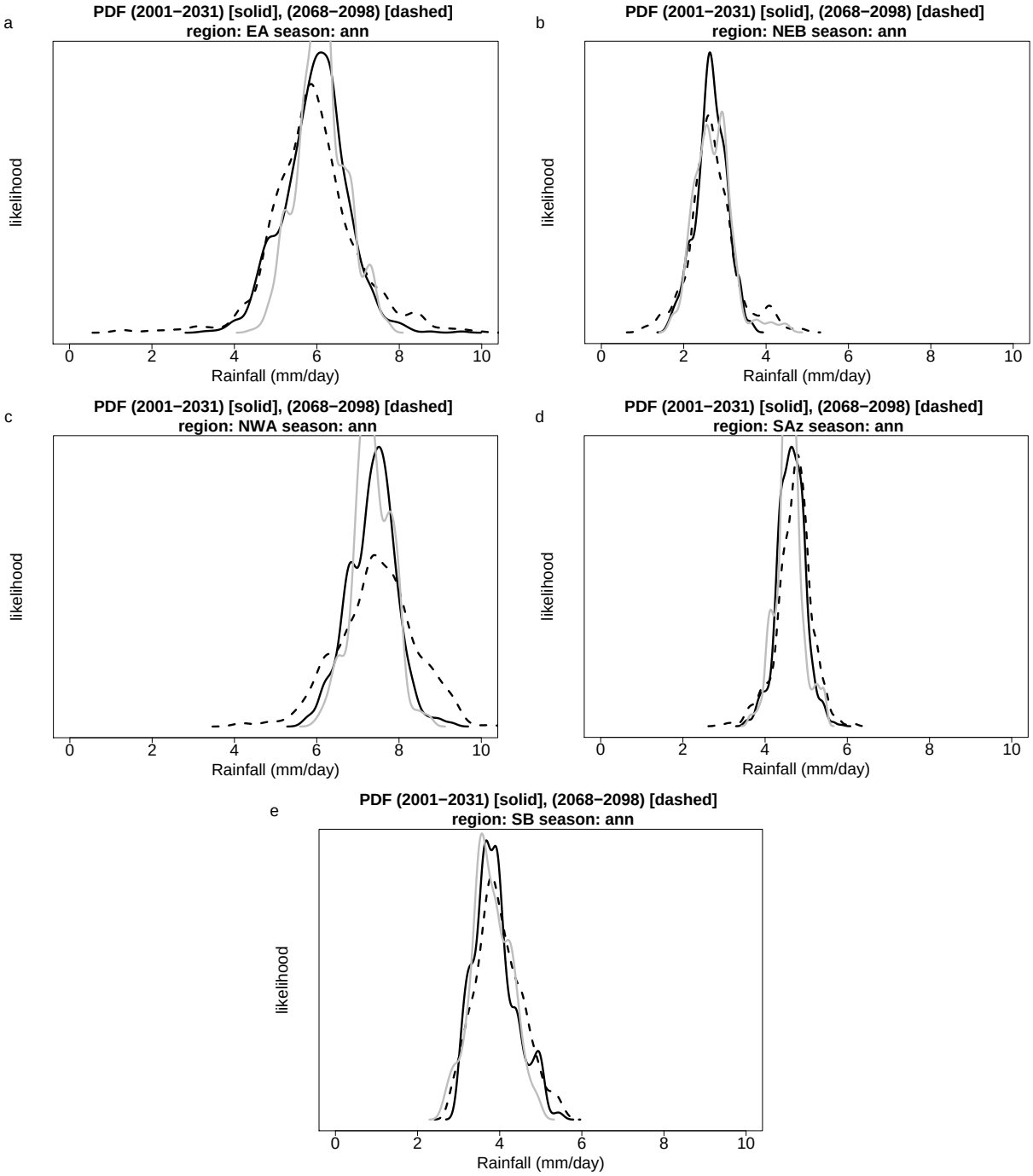

Figure 7: Changes in modelled rainfall PDFs between early twentieth century (2001–2031) and late twentieth century (2068–2098) (Table 1). Grey – observed distribution in twentieth century. Solid – predicted distribution in early twenty–first century. Dashed – predicted distribution in late twenty–first century. GCM predictions weighted according to the appropriate posterior distribution in Table 3.

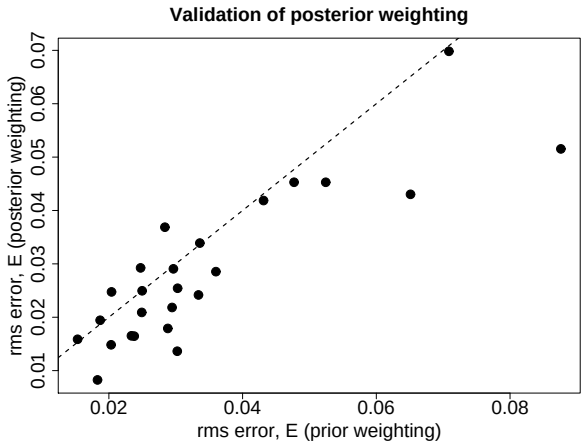

Figure 8: Comparison of rms error E in rainfall CDF for prior– and posterior–weighted predictions. Training period 1901–1959, validation period 1960–1999 (equation 9 with $x_1 = 0$ and $x_2 = 25$ mm day^{-1}). One data point for each season and each region. Dashed line has slope 1.